Low-high latitude forcing on the East Asian winter monsoon evolution since the last glacial maximum

Debo Zhao[1] , Shiming Wan[1,2] , Xinquan Zhou[3], Shoushu Jiang[1,4] and Anchun Li[1]

[1]Key Laboratory of Marine Geology and Environment, Institute of Oceanology, Chinese Academy of Sciences, Qingdao, China; [2]CAS Center for Excellence in Quaternary Science and Global Change, Xi'an, China; [3]State Key Laboratory of Marine Geology, Tongji University, Shanghai, China and [4]College of Marine Sciences, University of Chinese Academy of Sciences, Beijing, China

Abstract

The East Asian winter monsoon (EAWM) has a profound effect on the winter climate in East Asia. The modern EAWM variability is tightly linked to the high-latitude Northern Hemisphere climate change through the Siberian High and can also be regulated by the low-latitude El Niño-Southern Oscillation through oceanic or atmospheric teleconnections. However, the Quaternary EAWM evolution has long been only attributed to the high-latitude climate change, resulting in the uncertainty in interpreting the out-of-phased EAWM variation recording in the East Asian continent and marginal seas. Here we presented a sediment record at Integrated Ocean Drilling Program Site U1427 in the southern Japan Sea to reconstruct the EAWM evolution since the last glacial maximum. By combining our record with previous reconstructions and simulations, we found the synchronous relationship between winter monsoon in northern and southern regions of East Asia from ~24 to 8 ka, but anti-correlated relationship since ~8 ka. We proposed the winter insolation and Atlantic meridional overturning circulation were the main drivers from last glacial to early Holocene, and then ENSO became a dominant factor in controlling the regional heterogeneity of EAWM evolution in the middle and late Holocene. This research explains much of the controversy in the Quaternary EAWM records and highlights the low-high latitude interaction in East Asian winter climate change.

1. Introduction

The East Asian winter monsoon (EAWM) characterized by cold and dry northwesterlies over northern East Asia and marginal seas and northeasterlies above southern East Asia and South China Sea is a specific feature that could cause extreme frigid/warm winter weather or climate events, which give profound economical, biological and societal influences on this densely populated region (Chang *et al.* 2006; Gao *et al.* 2008; Wang *et al.* 2011). The modern EAWM variability is tightly linked to variations in northern high-latitude climate via the Siberian High (Chang & Lu, 2012; Zhang & Wang, 2020). On the other hand, low-latitude El Niño-Southern Oscillation (ENSO) can also regulate EAWM by modifying the atmospheric circulation over the western North Pacific (Geng *et al.* 2023; Son *et al.* 2014; Zhang *et al.* 2016).

The Quaternary EAWM intensity has been reconstructed extensively based on Chinese loess, lake and marine sediments (Hao *et al.* 2012; Huang *et al.* 2023; Jia *et al.* 2015; Kang *et al.* 2020; Li *et al.* 2017; Liu & Ding, 1998; Sun *et al.* 2012; Zhao *et al.* 2019; Zheng *et al.* 2014). However, these reconstructed monsoon variabilities and proposed forcing mechanisms remain under debate at multi-time scales. Especially, records have suggested inconsistent EAWM patterns between the northern and southern East Asia and its marginal seas (Hao *et al.* 2017; Huang, 2015; Huang *et al.* 2011; Huang *et al.* 2023; Liu *et al.* 2020; Steinke *et al.* 2011; Zheng *et al.* 2014), probably indicating the regional heterogeneity of EAWM evolution (Zhao *et al.* 2019). Studies have linked the winter solar insolation and the resultant variations in atmospheric circulation over East Asian continent and Pacific to the EAWM variation (Huang *et al.* 2023; Kutzbach, 1981; Wen *et al.* 2016). Changes in Northern Hemisphere ice volume and hemispheric temperature gradient have also been adopted as dominant factors (Hao *et al.* 2012; Kang *et al.* 2020). Besides, millennial scale of abrupt changes in EAWM during the last glaciation has been attributed to the Atlantic meridional overturning circulation (AMOC) reorganization (Liu *et al.* 2020; Sun *et al.* 2012). Nevertheless, all these proposed forcings cannot fully explain the observed regional heterogeneity of EAWM evolution.

The EAWM brings dry air-mass across the Asian continent but carries moisture when it flows across the warm Japan Sea. This moisturized wind brings much more snowfall and rainfall to the Japan Sea side of the Japanese Islands during winter than other seasons (Sone *et al.* 2013).
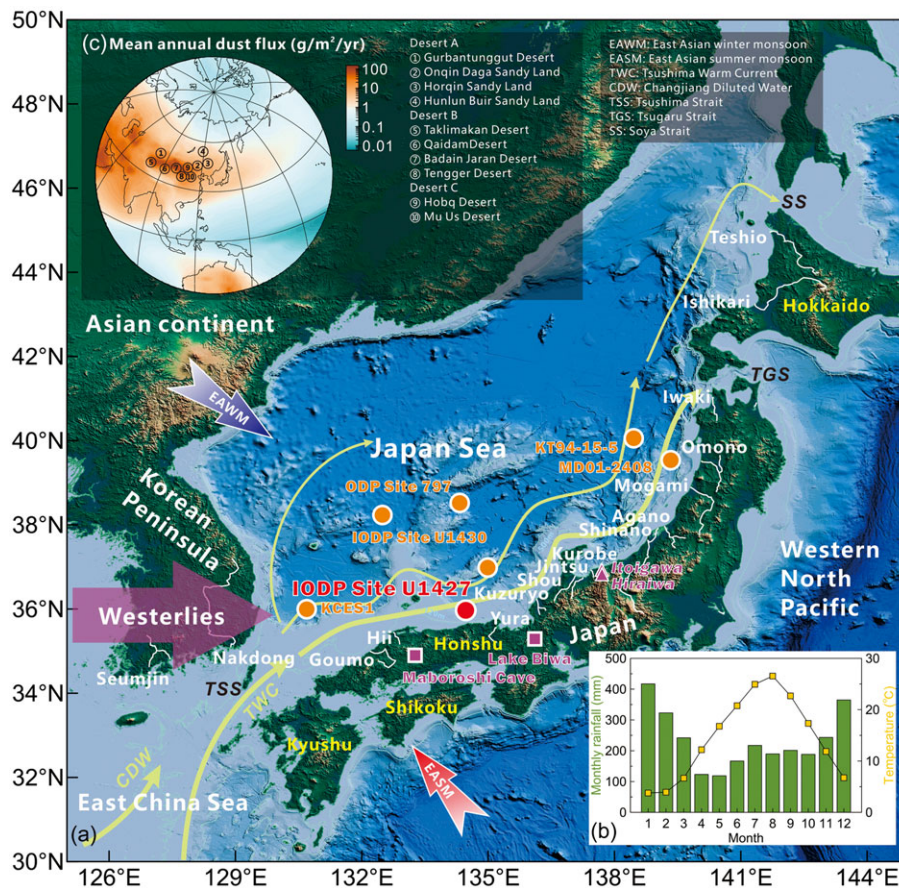
Figure 1. (Colour online) (a) Map showing the location of the IODP Site U1427 (red dots), bathymetry of the Japan Sea and the flow of surface currents (yellow arrow lines). The referenced ocean sites and lake pollen and speleothem records are shown with orange dots and purple squares, respectively. EAWM, EASM and Northern Hemisphere subtropical westerlies are shown with blue, red and purple arrows, respectively. White lines show rivers on the Japanese Islands. Abbreviations of East Asian monsoon, ocean currents and straits are also shown. (b) Monthly rainfall at the Hiraiwa Precipitation Observatory and temperature at Itoigawa (Sone *et al.* 2013) in the Japan Sea side of the Japanese Islands are shown with purple triangles in (a). (c) Mean annual dust flux in the Eurasia and North Pacific (Kok *et al.* 2021). Numbers show the deserts in the northern China, which were divided into three regions: Deserts A, B and C (Chen *et al.* 2007).

Such hydroclimate condition favours more sediment eroded from the island's input to the southern Japan Sea during winter than other seasons (Otosaka *et al.* 2004). Thus, the sediment records in this region could be the ideal candidates to reconstruct EAWM evolution. Here we present a high-resolution sediment record at Integrated Ocean Drilling Program (IODP) Site U1427 in the southern Japan Sea (Figure 1a). Grain-size analysis and Sr-Nd isotopic sediment source tracing have been used to trace the sediment supply from the island to Japan Sea and further reconstruct the EAWM evolution since the last glacial maximum (LGM). By comparing the EAWM in the northern and southern regions of East Asia and its marginal seas, we proposed that ENSO overwhelmed winter insolation and became the dominant factor in controlling the regional heterogeneity of long-term EAWM evolution through ocean-atmosphere interactions in the middle and late Holocene.

2. Study area

The Japan Sea is a back-arc basin in the northwestern Pacific bounded by the Eurasian continent, the Japanese Islands and Sakhalin Island, and connects to the East China Sea, Sea of Okhotsk

and North Pacific by shallow straits (Figure 1a). It has an average depth of 1350 m and a maximum depth of ~3700 m. Climatologically, the Japan Sea is influenced by the prevalent East Asian monsoon, consisting of the East Asian summer monsoon (EASM), characterized by warm and moist winds from the Pacific in boreal summer, and the EAWM, characterized by cold and dry air winds from the Siberian High in boreal winter (Tada *et al.* 2014).

Given the Tsushima Warm Current (TWC), a branch of the Kuroshio Current, flow into the Japan Sea through the Tsushima Strait (Figure 1a), the cold and dry northwesterly winter winds can be moistened and heated. Thus, the EAWM and the carried water vapour and heat over the Japan Sea are the major factors contributing to variations in snowfall and rainfall on the Japan Sea side of the Japanese Islands (Inoue *et al.* 2015; Takahashi, 2021; Takano *et al.* 2008). Instrumental record at Hiraiwa Precipitation Observatory near our study site suggest the rainfall during the EAWM months (from November to March) accounts for 59% of the annual precipitation (Sone *et al.* 2013) (Figure 1b). Such hydroclimate condition enhanced sediment erosion on the islands and thus results in higher sediment flux in Yamato Basin in the eastern Japan Sea during winter than summer (Otosaka *et al.* 2004).

Table 1. Radiocarbon dating and correlation points between reflectance b* and NGRIP $\delta^{18}O$

CSF-A Bottom depth (cm)	Species	Conventional AMS^{14}C age (yr BP)	Calendar age (cal. yr BP)	Reflectance b*	NGRIP $\delta^{18}O$
20	Planktonic foraminifer mixture	1800 ± 30	1213 ± 82	\	\
90	Planktonic foraminifer mixture	7260 ± 30	7568 ± 82	\	\
290	Planktonic foraminifer mixture	10360 ± 40	11396 ± 86	\	\
384	Planktonic foraminifer mixture	11220 ± 40	12602 ± 86	\	\
760	Planktonic foraminifer mixture	20410 ± 80	23605 ± 110	\	\
320	\	\	11620	4.00	−36.41
372	\	\	11940	−0.32	−41.94
420	\	\	14600	2.70	−35.81
498	\	\	15580	−1.66	−44.56
570	\	\	17100	0.80	−38.99
640	\	\	18560	−0.20	−39.92
676	\	\	19680	−0.72	−39.93
716	\	\	22160	−0.46	−41
736	\	\	23300	−0.60	−39.11

3. Material and methods

3.a. Core descriptions and chronological framework

IODP Site U1427 (35°57.92' N, 134°26.06' E, 330 m water depth) is located in the south-central part of the Japan Sea on the outer margin of the southeast-northwest trending continental shelf, ~35 km from the northern coast of Honshu Island (Tada *et al.* 2014) (Figure 1a). The lithologic composition of sediments is dominated by clayey silt and nannofossil- or biosiliceous-rich clayey silt. Centimetre-thick tephra layers occur frequently throughout the succession. The hole A of Site U1427 was cored to 548.6 m depth below seafloor, with a recovery of 542.59 m (98.9%). Here we focused on the top 7.75 m of the Hole A. No obvious tephra layers appear in this interval (Tada *et al.* 2014).

Chronological framework was established based on 5 accelerator mass spectrometry (AMS) ^{14}C dates measured by Beta Analytic Inc, in conjunction with correlations between reflectance b* (Tada *et al.* 2014) and NGRIP $\delta^{18}O$ record (Andersen *et al.* 2004). Radiocarbon dates were performed on mixed planktonic foraminifera from 5 fine-grained sediment layers (Table 1). All radiocarbon ages were calibrated using software CALIB based on the marine calibration dataset Marine 20 (Reimer & Stuiver, 2016) with an adjustment for a regional ^{14}C reservoir age ($\Delta R = -21 \pm 76$) (Yoneda *et al.* 2007). The reflectance b* of Site U1427 has been interpreted to reflect the ratio of biogenic to terrigenous input, and thus used to correlate with the benthic foraminiferal $\delta^{18}O$ to build the age model (Sagawa *et al.* 2018). The trend of sediment colour reflectance b* data of the study interval at Site U1427 closely follows the NGRIP $\delta^{18}O$ record (Figure 2). Here 9 horizons were correlated between sediment reflectance b* and NGRIP $\delta^{18}O$ (Figure 2, Table 1). Between age control points, ages were linearly interpolated assuming constant sedimentation rates. The established age model reveals that the sediments extend to approximately 23.81 ka BP, with an average sedimentation rate of about 32.5 cm/ka. This is similar to the sedimentation rate of a nearby piston core obtained during the pre-expedition site survey cruise, which suggests an average sedimentation rate of ~30 cm/ka (Tada *et al.* 2014).
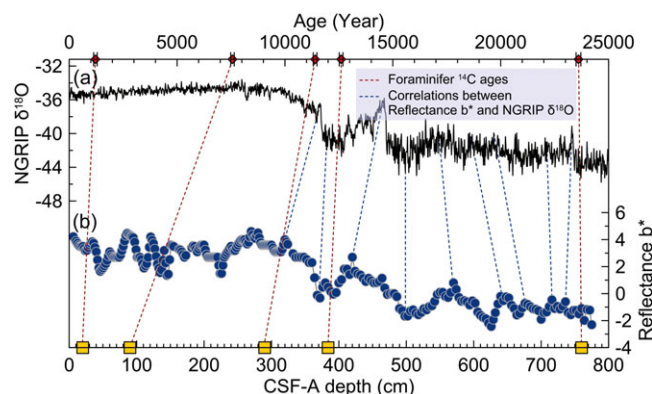

Figure 2. (Colour online) Age model of the top 7.75 m of the Hole A sediments at IODP Site U1427. The layers and their corresponding AMS ^{14}C dates are shown with yellow squares and red diamonds with black error bars, respectively, connected by red dotted lines. The blue dotted lines show the correlations between (a) NGRIP $\delta^{18}O$ and (b) sediment reflectance b*.

3.b. Analytical methods

A total of 266 samples from IODP Site U1427 were taken for the grain-size analysis. Samples were measured after removal of organic matter, carbonate and biogenic silica by hydrogen peroxide (15%), hydrochloric acid (0.5 mol/L) and sodium carbonate (2 mol/L), respectively (Zhao *et al.* 2018; Zhao *et al.* 2020). Grain-size measurements were carried out on a Cilas 1190 L apparatus in the laboratory of Institute of Oceanology, Chinese Academy of Sciences (IOCAS). The analytical range is from 0.04 to 2500 μm. The measurement repeatability of the instrument is 0.5%, and the reproducibility is better than 2%. Then unmixing of the yielded raw grain-size distributions into unimodal parametric end-members was performed by parametric end-member analysis (EMA) with skewed generalized Gaussian (SGG) distribution using the Matlab-based software package AnalySize (Paterson & Heslop, 2015; Zhao *et al.* 2020).

The bulk fine fractions of the samples (n = 9) were pretreated using the same procedure with grain-size analysis to remove the organic matter, carbonate and biogenic silica. Then, the 2–32 μm and 32–63 μm fractions were separated by wet-sieve and centrifugation. Further, the Sr-Nd isotope compositions of these two separated fractions were determined. The Sr-Nd isotope compositions were measured by Thermo Fisher Scientific Triton TIMS instrument at the laboratory of Tianjin Center, China Geological Survey, following the method described by (Tang et al. 2022). The standard Sr solution (NBS987) showed an average $^{87}Sr/^{86}Sr$ value of 0.710250 ± 4 (2σ) (n = 11, recommended value of 0.710250), and the standard Nd solution (JNdi-1) yielded an average $^{143}Nd/^{144}Nd$ value of 0.512111 ± 4 (2σ) (n = 11, recommend value of 0.512115). All measured $^{143}Nd/^{144}Nd$ and $^{87}Sr/^{86}Sr$ values were normalized to $^{146}Nd/^{144}Nd = 0.7219$ and $^{88}Sr/^{86}Sr = 0.1194$, respectively. Nd isotopic results are presented as $\varepsilon Nd = [((^{143}Nd/^{144}Nd)_{sample})/0.512638)-1] \times 10000$ (Jacobsen & Wasserburg, 1980).

4. Results

4.a. Grain-size end-member analysis

The goodness of fit statistics (coefficient of determination $r^2 > 90\%$, degree of angle < 5 for 3 end-members) shows that the three end-member model is the optimization (Figure 3a and b). These three end-member model contains grain-size modes of ~12 μm, ~32 μm and ~56 μm for end-members EM1, EM2 and EM3, respectively (Figure 3c). The end-member abundances for each end-member since LGM have been shown in Figure 3d. The EM1 suggests overall increased trends during ~24–17 ka and ~15–8 ka, and decreased trends during ~17–15 ka and since ~8 ka. Generally, the EM3 shows almost reverse relationship with EM1, but with low abundances during ~21–17 ka and ~10–7.5 ka. The EM2 also shows a reverse trend compared with EM1, except for several millennial scale of fluctuations during ~17.5–15 ka, ~12–10 ka and ~7.5–6.5 ka.

4.b. Sr-Nd isotopic composition

The Sr-Nd isotopic compositions are shown in Table 2. The 2–32 μm fraction has higher $^{87}Sr/^{86}Sr$ values (average 0.710883) than the 32–63 μm fraction (average 0.7079383), suggesting the grain-size effect on the Sr isotopic composition. This is mainly due to the coarse fractions are dominated by quartz and feldspar, with low $^{87}Sr/^{86}Sr$ values, whereas the fine fraction mainly contains clay minerals and micas, which are characterized by high $^{87}Sr/^{86}Sr$ ratios (Innocent et al. 2000; Meyer et al. 2011). Such grain-sized effect has also been observed in the previous studies of East Asian marginal sea sediments (Shen et al. 2017; Zhao et al. 2017). In contrast, Nd isotopes in sediments are not significantly influenced by erosion and transport compared to the original bedrock values (Zhao et al. 2017). The $\varepsilon_{Nd(0)}$ of the 2–32 μm fraction shows more negative values (average −6.4) than the 32–63 μm fraction (average −3.6), indicating their distinct sediment sources.

5. Discussion

5.a. Sediment provenance

A prerequisite for interpretation of mineralogical or geochemical trends in marine sediments is ascertaining their source areas (Colin

et al. 2006; Wan et al. 2015). IODP Site U1427 has multiple potential sediment sources including the deserts in central and eastern Asia, nearby islands and mainland Asia. Modern observation and modelling results suggest the Japan Sea is a region that is significantly affected by the eolian dust released from the Asian arid regions (Kok et al. 2021) (Figure 1c). Sediment source tracing studies also suggested that eolian dust from these regions transported by the westerlies and/or the EAWM is the most important source of sediments in the Japan Sea (Irino & Tada, 2003; Nagashima et al. 2007a; Nagashima et al. 2007b; Nagashima et al. 2013; Shen et al. 2017).

Surrounding rivers in Japan Arc, Korean Peninsula and Russian coast are other possible sources of sediments in the Japan Sea. Rivers in the Japan Sea side of the Japanese Islands (Figure 1a) deliver a total of about 10 million tons/year (Mt/yr) of suspended sediments to the study region (Milliman & Farnsworth, 2013). Nakdong and Seumjin Rivers in Korean Peninsula deliver 8 Mt/yr and 2 Mt/yr sediments to the Tsushima Strait, respectively (Milliman & Farnsworth, 2013), are also possible sources of the southern Japan Sea sediments. Sediment contribution from the Russian Tumnin and Zheltaya Rivers should be very minor because of their very low sediment discharge (<0.5 Mt/yr) (Milliman & Farnsworth, 2013) and the blocking effect of the northeastward current system in the Japan Sea (Figure 1a). Besides, fine-grained suspended sediments derived from the Chinese large rivers including Yangtze and Yellow River can also be transported to the southern part of the Japan Sea by the TWC (Nagashima et al. 2007b).

To identify the provenance of sediments at IODP Site U1427, $^{87}Sr/^{86}Sr$ versus $\varepsilon_{Nd(0)}$ diagrams of 2–32 μm and 32–63 μm fractions were plotted with fine- (Figure 4a) and coarse-grained (Figure 4b) data, respectively, from potential sources including Japanese rocks and river sediments, Asian deserts, Chinese Loess Plateau, Yangtze and Yellow Rivers in East Asia and Korean river. All the samples of 32–63 μm fraction plot within the range of Japanese end-member, indicating the dominant contribution of terrigenous materials eroded from Japan to this coarse fraction. This is reasonable because the nearshore location (~35 km from the coast) and higher sedimentation rate (~32.5 cm/ka) of IODP Site U1427 are compared with other offshore sites (e.g. IODP Site U1430 (Figure 1a), with an average sedimentation rate of ~3.9 cm/ka during the late Pleistocene (Shen et al. 2017)).

Almost all the samples of 2–32 μm fraction deviate from the Japanese end-member, but close to the Asian desert end-member, especially the Desert A group including Gurbantunggut Desert, Onqin Daga Sandy Land, Horqin Sandy Land and Hunlun Buir Sandy Land in relatively higher latitude (Figure 1a). This suggests the Desert A region probably contributes a large part of the sediments in the study region. An alternative explanation is that such Sr-Nd isotopic composition of 2–32 μm fraction can be caused by the mixing between Japanese end-member and Asian deserts, Chinese Loess Plateau, Yangtze and Yellow Rivers and Korean river. Observation during the Asian dust period at a Korean site suggests the eolian grain-size distribution is dominated by the mean diameter of 8.5 μm (Park & Kim, 2006), close to our 2–32 μm fraction. It has been proposed that the silt (>4 μm) population of Japan Sea sediments have been mostly supplied from the Asian arid regions by eolian dust transport (Nagashima et al. 2007b). Besides, grain-size end-member with the median grain size of 9.5 μm in the southwestern Japan Sea sediments has also been interpreted as the Asian dust source in a recent research (Bahk et al. 2021). Therefore, we tend
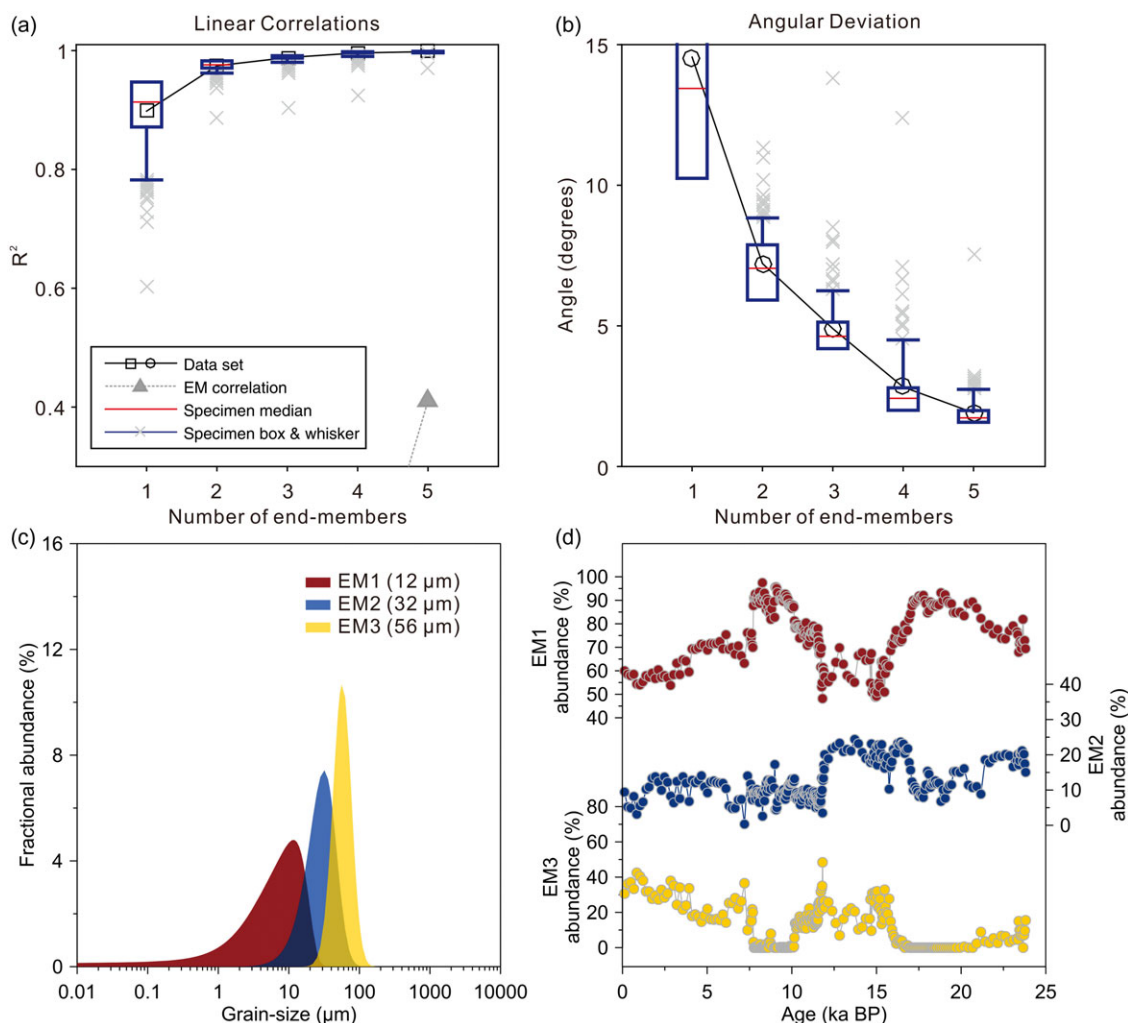
Figure 3. (Colour online) End-member modelling results of Site U1427 grain-size data. (a) Coefficients of determination (R^2) for each size class of models with 1–5 end-members. (b) Angular differences (in degrees) between the reconstructed and observed datasets as a function of the number of end-members. (c) Modelled three end-members of the terrigenous sediment fractions from Site U1427. (d) Variations of end-member abundances of EM1–EM3 during the last ~24 ka.

to interpret the 2–32 μm fraction as an eolian dust end-member, but probably can be disturbed by other source regions including Yangtze and Yellow Rivers and Korean river by the TWC intrusion (Nagashima *et al.* 2007b; Zou *et al.* 2021).

5.b. EAWM evolution in the northern East Asia and its marginal seas

Based on the source tracing results, variation of the 32–63 μm fraction in sediments at IODP Site U1427 can be regarded as the indicator of sediment supply from the Japanese Islands. It can be represented approximately with changes in the combined abundance of EM2 (median grain size of 32 μm) and EM3 (median grain size of 56 μm). To constrain the control mechanism of sediment supply from the Japanese Islands, we compared the abundances of EM2 and EM3 with the potential forcings including southwestern Japan rainfall, EAWM, EASM, sea surface temperature (SST) of the Japan Sea and sea level change (Figure 5).

Sediment input from the Japanese Islands was mainly linked to the land erosion controlled by local rainfall and snowfall, as well as

sea level change. The abundances of EM2 and EM3 are roughly coherent with the winter rainfall record based on pollen in Biwa Lake and speleothem $\delta^{18}O$ record from Maboroshi Cave, suggesting increased sediment supply under enhanced local rainfall (Figure 5a). It should be noted that this pollen record shows weak fluctuations during deglacial cold events, probably due to the long distance of Biwa Lake from Japan Sea. Despite the glacial depletion of Maboroshi Cave $\delta^{18}O$ was ascribed to changes in seasonality of precipitation, larger fractionation under lower temperature or a longer vapour trajectory due to exposed sea shelf, the almost anti-phased relationship between Maboroshi and Chinese cave $\delta^{18}O$ record, which also received water vapour generated in lower glacial temperature across the wide exposed sea shelf, indicating increased seasonal rainfall (weakened EASM but enhanced EAWM rainfall (Figure 5a and d)) probably was the main reason of $\delta^{18}O$ variation in southwestern Japan. Basically, rainfall in the Japan Sea side of the Japanese Islands mainly depends on EAWM and SST of the Japan Sea. Modern observation data suggest that anomalous high SSTs in the Japan Sea can strengthen the upward heat and moisture flux and the air-mass modification, and thus significantly related to the rainfall or

Table 2. Sr-Nd isotopic composition of 2–32 μm and 32–63 μm fractions in IODP Site U1427 sediments

Samples sites	Depth (cm)	Age (ka BP)	$^{87}Sr/^{86}Sr$ ($\pm 2\sigma \times 10^{-6}$)	$^{143}Nd/^{144}Nd$ ($\pm 2\sigma \times 10^{-6}$)	$\varepsilon_{Nd(0)}$ ($\pm 2\sigma$)
2–32 μm	20	1.21	0.710784 ± 9	0.512267 ± 5	−7.2 ± 0.10
	90	7.57	0.710080 ± 9	0.512314 ± 7	−6.3 ± 0.14
	151	8.73	0.710326 ± 3	0.512418 ± 6	−4.3 ± 0.12
	220	10.05	0.711259 ± 6	0.512283 ± 4	−6.9 ± 0.08
	290	11.38	0.711545 ± 5	0.512272 ± 7	−7.1 ± 0.14
	380	12.38	0.710471 ± 6	0.512310 ± 4	−6.4 ± 0.08
	460	15.1	0.710499 ± 7	0.512302 ± 6	−6.6 ± 0.12
	660	19.18	0.711576 ± 3	0.512314 ± 9	−6.3 ± 0.18
	760	23.61	0.711411 ± 6	0.512309 ± 7	−6.4 ± 0.14
32–63 μm	20	1.21	0.708209 ± 8	0.512419 ± 9	−4.3 ± 0.18
	90	7.57	0.708038 ± 7	0.512408 ± 9	−4.5 ± 0.18
	151	8.73	0.707319 ± 7	0.512513 ± 2	−2.4 ± 0.04
	220	10.05	0.708151 ± 4	0.512430 ± 8	−4.1 ± 0.16
	290	11.38	0.707659 ± 7	0.512446 ± 8	−3.7 ± 0.16
	380	12.38	0.707689 ± 2	0.512454 ± 7	−3.6 ± 0.14
	460	15.1	0.708065 ± 3	0.512461 ± 9	−3.5 ± 0.18
	660	19.18	0.708288 ± 7	0.512440 ± 5	−3.9 ± 0.10
	760	23.61	0.708027 ± 8	0.512490 ± 6	−2.9 ± 0. 12

snowfall on the island (Sone *et al.* 2013; Takano *et al.* 2008). However, the distinct relationship between sediment input reconstructed with abundances of EM2 and EM3 and Japan Sea SST record indicates their weak links (Figure 5a and c). Besides, the warming-induced spring melting of winter snow can also cause higher sediment supply. However, our results are not consistent with the Japan Sea SST record, suggesting that the temperature-induced melting is not the first controlling factor of sediment supply (Figure 5a and c). Generally, the EM2 and EM3 abundances suggest a similar trend compared with the EAWM records in the Chinese Loess Plateau, Okinawa Trough and Yellow Sea, as well as the model simulation (Figure 5a and b), indicating the strong control of EAWM on local rainfall and sediment input from the island to Japan Sea.

Almost anti-phased relationship between EM2 and EM3 abundances and EASM suggests the insignificant roles of EASM in sediment supply from the Japanese Islands (Figure 5a and d). The westerlies can also have an impact on local rainfall through the East Asian Meiyu-Baiu fronts. However, our study region is located on the northern edge of the Meiyu-Baiu fronts, which receive its effects in July (Li *et al.* 2018). This only results in a slight increase in local rainfall during summer season (Figure 1b). Therefore, the meridional shifts of westerlies should have less influence on local hydroclimate compared to the EAWM. Besides, the water depth (~330 m) of our study site is beyond the sea level fluctuation range (~120 m) during glacial-interglacial cycles. Combined with the narrow shelf of Honshu Island (Figure 1a), the estuary advances and retreats along with sea level changes should have small effects on the terrestrial materials input to the Japan Sea. This can be verified by the

absence of negative relationship between sea level change and EM2 and EM3 abundances since the LGM (Figure 5a and e). It should be noted that deglacial rapid sea level rise-induced sediment reworking probably also contributes to increased EM2 and EM3 abundances from ~15 to 10 ka (Figure 5a and e). Enhanced anthropogenic activities, e.g. agriculture, have also been proposed as a strong force in driving land weathering and erosion (Pei *et al.* 2023). However, large scale of population increases and agriculture activities in Japan mainly started after 3 ka BP (Crawford, 2011; Mizuno *et al.* 2021) and thus probably contributed only a small part of increasing in sediment supply from Honshu Island to the Japan Sea since the early Holocene.

As a result, the grain-size index of EM2 and EM3 abundance was interpreted as an EAWM proxy in the Japan Sea. Combined with other EAWM records, we found the EAWM in the northern East Asia and its marginal seas suggest weakened long-term trend during ~24–17.5 ka and ~11.8–8 ka and strengthened during ~17.5–15 ka and since ~8 ka. On the millennial scale, an intensified EAWM was found during the Heinrich 1 (H1) and Younger Dryas (YD) cooling events and weakened during the Bølling-Allerød (B-A) warming event (Figure 5a and b).

5.c. High-low latitude interaction forcing on the EAWM

To investigate the regional heterogeneity of EAWM evolution and its forcing mechanisms since the LGM, the EAWM records in the northern regions of East Asia and marginal seas have been compared with that in the South China Sea, Northern Hemisphere winter insolation, NGRIP δ^{18}O record and low-latitude ENSO records (Figure 6a–d). A striking phenomenon is
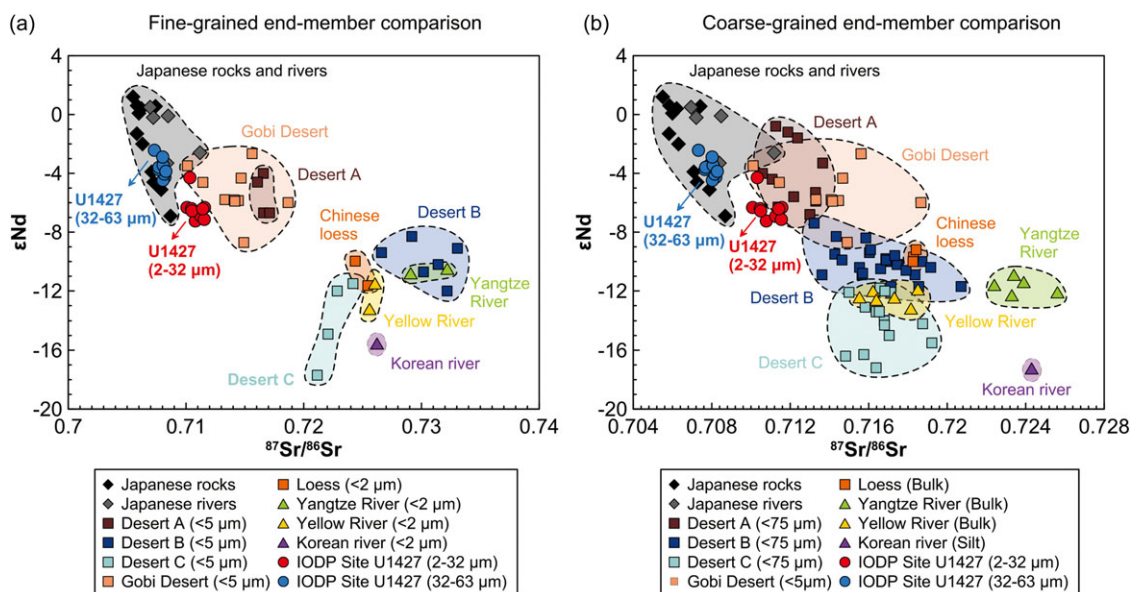
Figure 4. (Colour online) Provenance of 2–32 µm and 32–63 µm fractions from Site U1427 sediments based on the Sr-Nd isotopic composition. (a) Comparison with fine-grained end-members of potential source areas. (b) Comparison with coarse-grained end-members of potential source areas. Data sources: Japanese rivers (Goldstein & Jacobsen, 1988; Shen *et al.* 2017), Japanese rocks (Kagami *et al.* 1992), Deserts A, B and C (Chen *et al.* 2007), Gobi Desert (Biscaye *et al.* 1997; Zhao *et al.* 2015), Chinese loess (Chen *et al.* 2007; Zhao *et al.* 2017), Yangtze River (Meng *et al.* 2008; Yang *et al.* 2007; Zhao *et al.* 2017), Yellow River (Hu *et al.* 2012; Meng *et al.* 2008; Zhao *et al.* 2017), Korean river (Lee *et al.* 2008; Lim *et al.* 2015).

that the northern and southern EAWM records exhibit the same evolvement both on the long-term trend and millennial scale from the LGM to ~8 ka, but towards the anti-phased relationship with a strengthened northern EAWM but weakened one in the southern region since ~8 ka.

The long-term trend evolution of EAWM can be linked to the winter solar insolation (Huang *et al.* 2011; Huang *et al.* 2023; Wen *et al.* 2016). As perihelion shifts from boreal summer to winter, the insolation is reduced in the Northern Hemisphere in winter. This leads to a cooling and higher pressure over the East Asian continent relative to the surrounding oceans and thus a stronger northerly wind. Both the northern and southern EAWMs are generally anti-correlated with the winter insolation before ~8 ka (Figure 6a–c). After ~8 ka, the increased winter insolation probably also plays a role in controlling the weakened southern EAWM but cannot explain the strengthened northern EAWM (Figure 6a–c). Such strengthened northern EAWM since the early Holocene has been recently interpreted with the increased meridional temperature gradient between the Siberian High and Equatorial Low (Kang *et al.* 2020).

On the millennial scale, the intensified Northern and southern EAWMs during cold H1 and YD events were coeval with the shutdown or a reduction in strength of the AMOC (Figure 6a–c), indicating a strong linkage between the AMOC and the EAWM through changes in the meridional temperature gradient and Northern Hemisphere westerlies (Huang *et al.* 2011; Sun *et al.* 2012). However, the northern and southern EAWMs were all not strong enough as expected during the LGM but went for a maximum until the deglacial (Figure 6b and c). Actually, such relatively weak EAWM during LGM compared to deglacial has also been found in the Gulang (Sun *et al.* 2012) and Luochuan (Hao *et al.* 2012) loess section in Chinese Loess Plateau within dating uncertainties. The relatively stronger AMOC strength during LGM compared to that during H1 and YD events (Huang *et al.* 2011), combined with the high winter insolation during this period probably accounted for such weak EAWM condition.

However, the anti-phased relationship between the northern and southern EAWM can hardly be explained by the insolation and/or northern high-latitude climate forcing (Figure 6b and c). Here we introduced the low-latitude ENSO processes to explain such regional heterogeneity. A modern climate modelling with CCSM3 suggested that a mature phase of El Niño in winter would lead to a strengthened EAWM over the northern East Asia but a weakened one over the south, through the reversed anomalous geopotential height and wind anomalies between the northeastern regions of East Asia and South China Sea, respectively (Sun & Yang, 2005). Recently, such modes among ENSO, cyclone/anticyclones and EAWM system have also been found during the midwinter based on observational and reanalysis datasets (Geng *et al.* 2023) (Figure 6e and f). During the El Niño midwinter, the abrupt North Atlantic Oscillation (NAO) phase transition from positive to negative leads to a rapid adjustment of the mid-latitude atmospheric circulation via wave eastward propagation along the mid-latitude jet. This leads to a strengthened Siberian high, combined with the anomalously negative geopotential height centred over the northeastern part of East Asian marginal seas, producing northwesterly wind anomalies and thus strong EAWM over northern East Asia (Figure 6f), which bring enhanced rainfall and snowfall in the Japan Sea and the Japan Sea side of the Japanese Islands (Figure 6e). In contrast, the anomalous Philippine Sea anticyclone shifts southward and results in the anomalous southwesterlies, and thus a weakened EAWM in the South China Sea.

Such ENSO-EAWM mode can well explain the observed anti-phased relationship between northern and southern EAWMs since ~8 ka. Enhanced El Niño amplitude since ~8 ka resulted in a strengthened northern EAWM but a weakened southern EAWM (Figure 6b–d). This low-latitude ENSO forcing on the regional heterogeneity of EAWM evolution has also been proposed in a previous study in the northern Okinawa Trough (Zhao *et al.* 2019). Even the El Niño amplitude also enhanced during the LGM, H1 and YD periods,
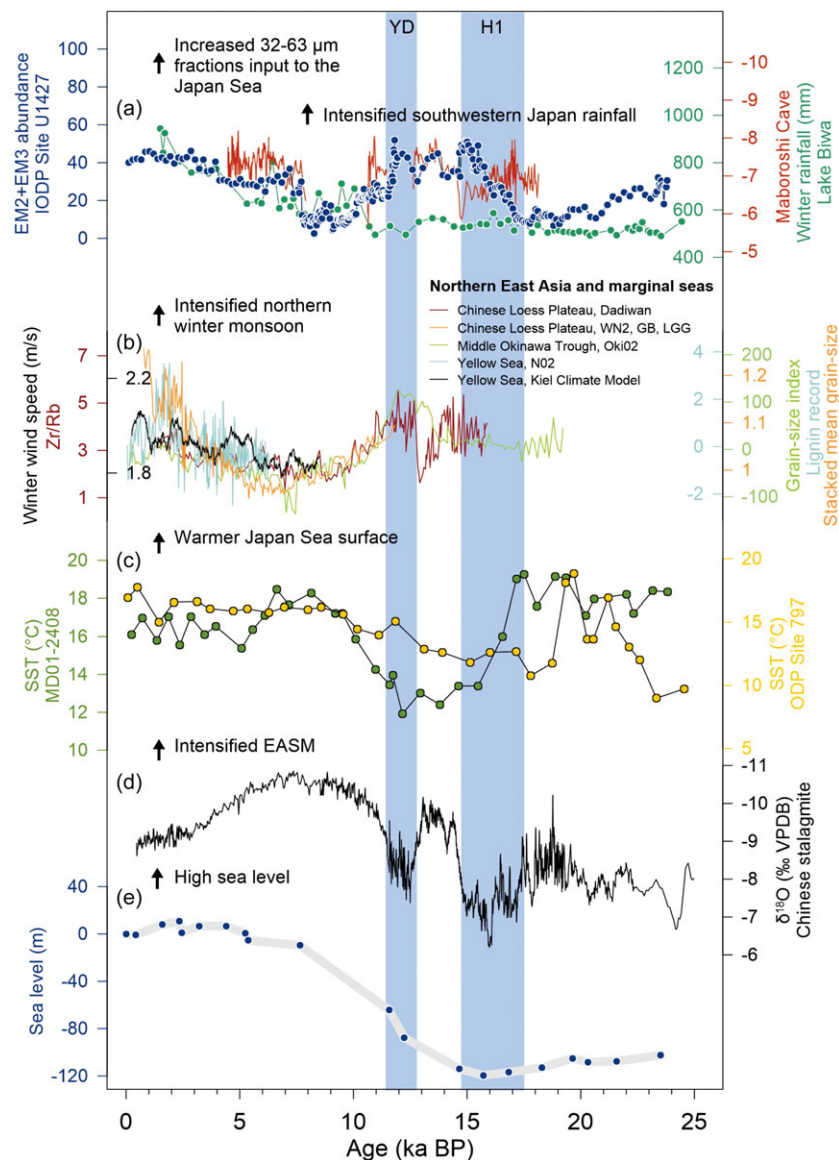
Figure 5. (Colour online) Comparison between (a) Japanese sediment input index established with EM1 and EM2 abundances with speleothem δ¹⁸O record from the Maboroshi Cave (Kato *et al.* 2021) and winter rainfall record in Lake Biwa (Kigoshi *et al.* 2014), and (b) EAWM (Hao *et al.* 2017; Kang *et al.* 2020; Liu *et al.* 2020; Zhao *et al.* 2019; Zheng *et al.* 2014), (c) Japan Sea SST (Fujine *et al.* 2009; Liu *et al.* 2014a), (d) EASM (Cheng *et al.* 2016) and (e) sea level change (Saito *et al.* 1998). The blue bars show the intervals of YD and H1.

we proposed that the North Atlantic climate signals were strong enough in dominating the EAWM system, and thus produced the coherent variations of EAWMs in the entire regions of East Asia and marginal seas (Figure 6b–d). In the context of global warming, increased frequency of extreme El Niño and La Niña events will very likely enlarge the spatial discrepancies of EAWM intensities (Cai *et al.* 2014; Cai *et al.* 2015) and lead to higher frequencies of extremely cold/warm winter in this region. Our findings highlight the role of tropical forcing in East Asian climate change through ocean-atmosphere interactions and have important implications for future projections of winter climate in this densely populated region.

6. Conclusion

Based on the sediment input from the Japanese Islands to the southern Japan Sea, we reconstruct the history of the EAWM in the northern East Asian marginal sea since the LGM. We found a synchronous relationship between winter monsoons in northern and southern regions of East Asia from ~24 to 8 ka, but anti-correlated relationship since ~8 ka. We proposed the winter insolation and AMOC were the main drivers for the long-term and millennial scale of variations from last glacial to early Holocene, and then ENSO became a dominant factor in controlling the regional heterogeneity of EAWM evolution through ocean-atmosphere interactions in the middle and late Holocene.
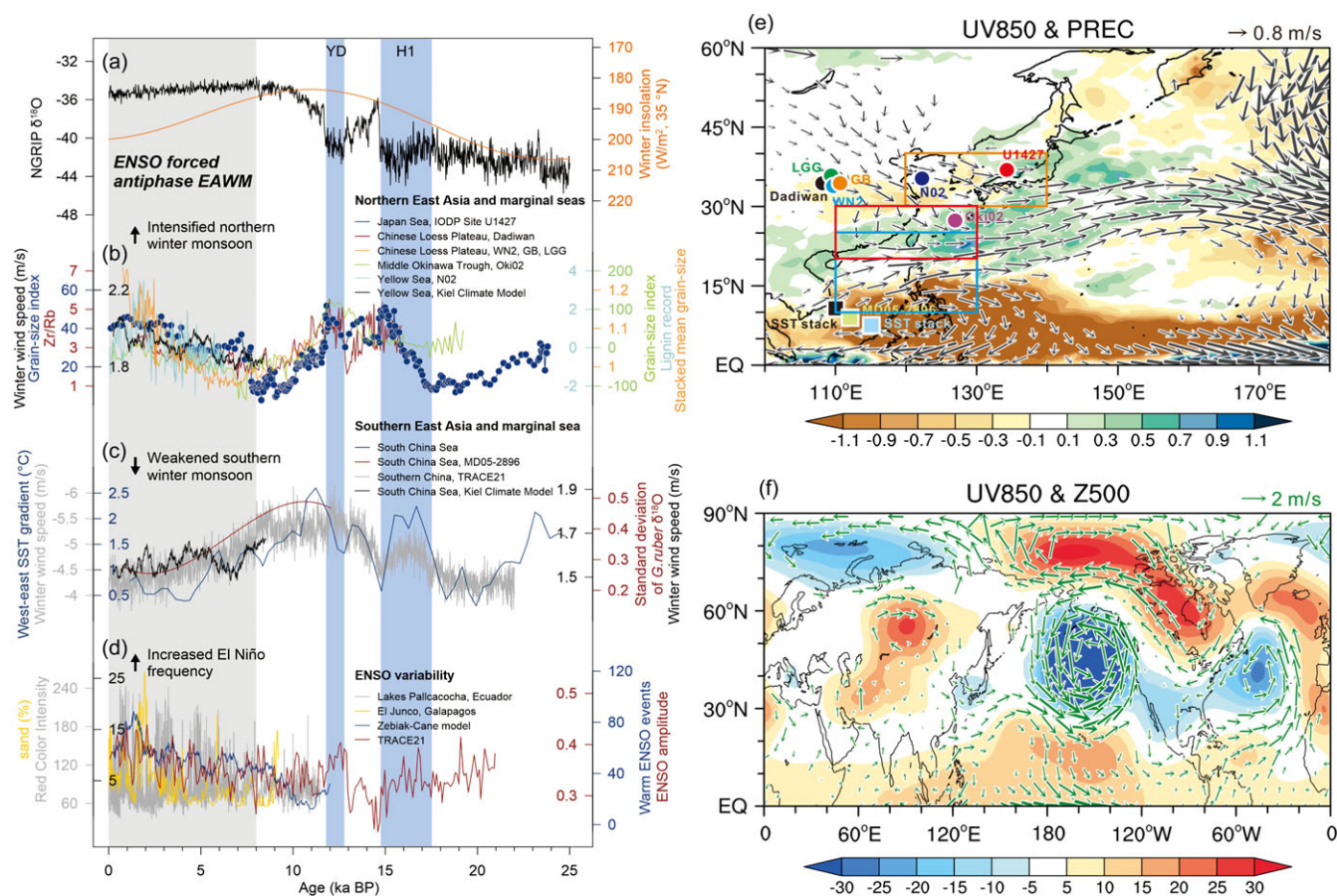
Figure 6. (Colour online) Comparison between EAWM with its potential forcing mechanisms. (a) NGRIP δ¹⁸O record (Andersen *et al.* 2004) and winter insolation in 35°N (Laskar *et al.* 2004). (b) EAWM reconstructions and simulation in the northern East Asia and its marginal seas. (c) EAWM reconstructions and simulation in the southern China and South China Sea (Huang *et al.* 2011; Huang *et al.* 2023; Wen *et al.* 2016; Zhao *et al.* 2019). (d) ENSO reconstructions and simulation (Clement *et al.* 2000; Conroy *et al.* 2008; Liu *et al.* 2014b; Moy *et al.* 2002). (e) Regression coefficients of the 850-hPa wind (vectors in m/s) and rainfall anomalies (shadings in mm/day) with respect to the December, January and February (DJF) mean Niño-3.4 index for the midwinter (Geng *et al.* 2023). The EAWM records in the northern and southern regions are shown with dots and squares, respectively. Orange, red and blue boxes show the regions of model simulation. (f) Regression coefficients of the 850-hPa wind (vectors in m/s) and 500-hPa geopotential height anomalies (shadings in m) with respect to the DJF mean Niño-3.4 index for the midwinter (Geng *et al.* 2023).

References

Andersen KK, Azuma N, Barnola JM, Bigler M, Biscaye P, Caillon N, Chappellaz J, Clausen HB, Dahljensen D and Fischer H (2004) High-resolution record of Northern Hemisphere climate extending into the last interglacial period. *Nature* **431**, 147–51.

Bahk J-J, Um I-K and Jang J-H (2021) Lateral sediment transport and late Quaternary changes of eolian sedimentation in the East Sea (Japan Sea). *Journal of Asian Earth Sciences* **208**, 104672.

Biscaye PE, Grousset FE, Revel M, Gaast S V. D., Zielinski, G. A., Vaars, A. and Kukla, G. J. (1997) Asian provenance of glacial dust (stage 2) in the Greenland ice sheet project 2 ice core, summit, Greenland. *Journal of Geophysical Research: Oceans* **102**, 26765–81.

Cai W, Borlace S, Lengaigne M, Rensch PV, Collins M, Vecchi G, Timmermann A, Santoso A, Mcphaden MJ and Wu L (2014) Increasing frequency of extreme El Nino events due to greenhouse warming. *Nature Climate Change* **4**, 111–16.

Cai W, Wang G, Santoso A, Mcphaden MJ, Wu L, Jin FF, Timmermann A, Collins M, Vecchi G and Lengaigne M (2015) Increased frequency of extreme La Nina events under greenhouse warming. *Nature Climate Change* **5**, 132–37.

Chang C-P and Lu M-M (2012) Intraseasonal predictability of Siberian high and East Asian winter monsoon and its interdecadal variability. *Journal of Climate* **25**, 1773–78.

Chang CP, Wang Z and Hendon H (2006) The Asian winter monsoon. In *The Asian Monsoon* (ed B. Wang), pp. 89–127. Berlin, Heidelberg: Springer Berlin Heidelberg.

Chen J, Li G, Yang J, Rao W, Lu H, Balsam W, Sun Y and Ji J (2007) Nd and Sr isotopic characteristics of Chinese deserts: implications for the provenances of Asian dust. *Geochimica Et Cosmochimica Acta* **71**, 3904–14.

Cheng H, Edwards RL, Sinha A, Spötl C, Liang Y, Chen S, Kelly M, Kathayat G, Wang X and Li X (2016) The Asian monsoon over the past 640,000 years and ice age terminations. *Nature* **534**, 640–46.

Clement AC, Seager R and Cane MA (2000) Suppression of El Niño during the Mid-Holocene by changes in the Earth's orbit. *Paleoceanography* **15**, 731–37.

Colin C, Turpin L, Blamart D, Frank N, Kissel C and Duchamp S (2006) Evolution of weathering patterns in the Indo-Burman Ranges over the last 280 kyr: effects of sediment provenance on $^{87}Sr/^{86}Sr$ ratios tracer. *Geochemistry, Geophysics, Geosystems* **7**, Q03007.

Conroy JL, Overpeck JT, Cole JE, Shanahan TM and Steinitz-Kannan M (2008) Holocene changes in eastern tropical Pacific climate inferred from a Galaˊpagos lake sediment record. *Quaternary Science Reviews* **27**, 1166–80.

Crawford GW (2011) Advances in Understanding Early Agriculture in Japan. *Current Anthropology* **52**(S4), S331–S345.

Fujine K, Tada R and Yamamoto M (2009) Paleotemperature response to monsoon activity in the Japan Sea during the last 160kyr. *Palaeogeography, Palaeoclimatology, Palaeoecology* **280**, 350–60.

Gao H, Chen L, Jia X, Ke Z, Han R, Zhang P, Wang Q, Sun C H, Zhu, Y, Li, W, Sun, L, Ren, F, Wang, L and Gao, G (2008) Analysis of the severe cold surge, ice-snow and frozen disasters in South China during January 2008:. possible climatic causes. *Meteorological Monthly* **4**, 014.

Geng X, Noh K-M, Kim K and Kug J-S (2023) Midwinter breakdown of ENSO climate impacts in East Asia. *npj Climate and Atmospheric Science* **6**, 155.

Goldstein SJ and Jacobsen SB (1988) Rare earth elements in river waters. *Earth and Planetary Science Letters* **89**, 35–47.

Hao, Q., Wang, L., Oldfield, F., Peng, S., Qin, L., Song, Y., Xu, B., Qiao, Y., Bloemendal, J. and Guo, Z. (2012) Delayed build-up of Arctic ice sheets during 400,000-year minima in insolation variability. *Nature* **490**, 393.

Hao T, Liu X, Ogg J, Liang Z, Xiang R, Zhang X, Zhang D, Zhang C, Liu Q and Li X (2017) Intensified episodes of East Asian Winter Monsoon during the middle through late Holocene driven by North Atlantic cooling events: high-resolution lignin records from the South Yellow Sea, China. *Earth & Planetary Science Letters* **479**, 144–55.

Hu B, Li G, Li J, Bi J, Zhao J and Bu R (2012) Provenance and climate change inferred from Sr–Nd–Pb isotopes of late Quaternary sediments in the Huanghe (Yellow River) Delta, China. *Quaternary Research* **78**, 561–71.

Huang E (2015) A comparison of the East Asian winter monsoon reconstructions from terrestrial and marine sedimentary records since the Mid-Pleistocene. *Quaternary Science* **35**, 1331–41.

Huang E, Tian J and Steinke S (2011) Millennial-scale dynamics of the winter cold tongue in the southern South China Sea over the past 26ka and the East Asian winter monsoon. *Quaternary Research* **75**, 196–204.

Huang E, Wang S, Wei S, Yuan Z and Tian J (2023) Precession control of interglacial winter monsoon intensity over tropical East Asia. *Global and Planetary Change* **229**, 104247.

Innocent C, Fagel N and Hillaire-Marcel C (2000) Sm-Nd isotope systematics in deep-sea sediments: clay-size versus coarser fractions. *Marine Geology* **168**, 79–87.

Inoue T, Kibe A, Ueda H and Mika S (2015) Snowfall variations in Japan and its linkage with tropical forcing. *International Journal of Climatology* **35**, 991–8.

Irino T and Tada R (2003) High-resolution reconstruction of variation in aeolian dust (Kosa) deposition at ODP site 797, the Japan Sea, during the last 200 ka. *Global and Planetary Change* **35**, 143–56.

Jacobsen SB and Wasserburg GJ (1980) Sm-Nd isotopic evolution of chondrites. *Earth and Planetary Science Letters* **50**, 139–55.

Jia G, Bai Y, Yang X, Xie L, Wei G, Ouyang T, Chu G, Liu Z and Peng PA (2015) Biogeochemical evidence of Holocene East Asian summer and winter monsoon variability from a tropical maar lake in southern China. *Quaternary Science Reviews* **111**, 51–61.

Kagami H, Iizumi S, Tainosho Y and Owada M (1992) Spatial variations of Sr and Nd isotope ratios of Cretaceous-Paleogene granitoid rocks, Southwest Japan Arc. *Contributions to Mineralogy and Petrology* **112**, 165–77.

Kang S, Du J, Wang N, Dong J, Wang D, Wang X, Qiang X and Song Y (2020) Early holocene weakening and mid- to late Holocene strengthening of the East Asian winter monsoon. *Geology* **48**, 1043–47.

Kato H, Amekawa S, Hori M, Shen CC, Kuwahara Y, Senda R and Kano A (2021) Influences of temperature and the meteoric water $\delta^{18}O$ value on a stalagmite record in the last deglacial to middle Holocene period from southwestern Japan. *Quaternary Science Reviews* **253**, 106746.

Kigoshi T, Kumon F, Hayashi R, Kuriyama M, Yamada K and Takemura K (2014) Climate changes for the past 52 ka clarified by total organic carbon concentrations and pollen composition in Lake Biwa, Japan. *Quaternary International* **333**, 2–12.

Kok JF, Adebiyi AA, Albani S, Balkanski Y, Checa-Garcia R, Chin M, Colarco PR, Hamilton DS, Huang Y, Ito A, Klose M, Leung DM, Li L, Mahowald NM, Miller RL, Obiso V, Pérez García-Pando C, Rocha-Lima A, Wan JS and Whicker CA (2021) Improved representation of the global dust cycle using observational constraints on dust properties and abundance. *Atmospheric Chemistry and Physics* **21**, 8127–67.

Kutzbach JE (1981) Monsoon climate of the early holocene: climate experiment with the earth's orbital parameters for 9000 years ago. *Science* **214**, 59–61.

Laskar J, Robutel P, Joutel F, Gastineau M, Correia ACM, Correia ACM and Levrard B (2004) A long-term numerical solution for the insolation quantities of the Earth. *Astronomy and Astrophysics* **428**, 261–85.

Lee SG, Kim JK, Yang DY and Kim JY (2008) Rare earth element geochemistry and Nd isotope composition of stream sediments, south Han River drainage basin, Korea. *Quaternary International* **176**, 121–34.

Li D, Zhao M and Tian J (2017) Low-high latitude interaction forcing on the evolution of the 400 kyr cycle in East Asian winter monsoon records during the last 2.8 Myr. *Quaternary Science Reviews* **172**, 72–82.

Li Y, Deng Y, Yang S and Zhang H (2018) Multi-scale temporospatial variability of the East Asian Meiyu-Baiu fronts: characterization with a suite of new objective indices. *Climate Dynamics* **51**, 1659–70.

Lim D, Jung H, Xu Z, Jeong K and Li T (2015) Elemental and Sr-Nd isotopic compositional disparity of riverine sediments around the Yellow Sea: constraints from grain-size and chemical partitioning. *Applied Geochemistry* **63**, 272–81.

Liu T and Ding Z (1998) Chinese loess and the paleomonsoon. *Annual Review of Earth & Planetary Sciences* **26**, 111–45.

Liu X, Sun Y, Vandenberghe J, Cheng P, Zhang X, Gowan EJ, Lohmann G and An Z (2020) Centennial- to millennial-scale monsoon changes since the last deglaciation linked to solar activities and North Atlantic cooling. *Clim. Past* **16**, 315–24.

Liu Y, Chen J, Chen J, Xing L, Zou J and Yao Z (2014a) Variations of alkenone temperature in the Sea of Japan during the last 170 ka and its paleoceanographic implications. *Chinese Science Bulletin* **59**, 4498–509.

Liu Z, Lu Z, Wen X, Otto-Bliesner BL, Timmermann A and Cobb KM (2014b) Evolution and forcing mechanisms of El Niño over the past 21,000 years. *Nature* **515**, 550–53.

Meng X, Liu Y, Shi X and Dewen DU (2008) Nd and Sr isotopic compositions of sediments from the Yellow and Yangtze Rivers: implications for partitioning tectonic terranes and crust weathering of the Central and Southeast China. *Frontiers of Earth Science in China* **2**, 418–26.

Meyer I, Davies GR and Stuut JBW (2011) Grain size control on Sr-Nd isotope provenance studies and impact on paleoclimate reconstructions: an example from deep-sea sediments offshore NW Africa. *Geochemistry, Geophysics, Geosystems* **12**, Q03005.

Milliman JD and Farnsworth KL (2013) *River discharge to the coastal ocean: a global synthesis*. Cambridge University Press.

Mizuno F, Gojobori J, Kumagai M, Baba H, Taniguchi Y, Kondo O, Matsushita M, Matsushita T, Matsuda F, Higasa K, Hayashi M, Wang L, Kurosaki K and Ueda S (2021) Population dynamics in the Japanese Archipelago since the Pleistocene revealed by the complete mitochondrial genome sequences. *Scientific Reports* **11**, 12018.

Moy CM, Seltzer GO, Rodbell DT and Anderson DM (2002) Variability of El Niño/Southern Oscillation activity at millennial timescales during the Holocene epoch. *Nature* **420**, 162–5.

Nagashima K, Tada R, Matsui H, Irino T, Tani A and Toyoda S (2007a) Orbital- and millennial-scale variations in Asian dust transport path to the Japan Sea. *Palaeogeography, Palaeoclimatology, Palaeoecology* **247**, 144–61.

Nagashima K, Tada R, Tani A, Toyoda S, Sun Y and Isozaki Y (2007b) Contribution of aeolian dust in Japan Sea sediments estimated from ESR signal intensity and crystallinity of quartz. *Geochemistry, Geophysics, Geosystems* **8**, Q02Q04.

Nagashima K, Tada R and Toyoda S (2013) Westerly jet-East Asian summer monsoon connection during the Holocene. *Geochemistry Geophysics Geosystems* **14**, 5041–53.

Otosaka S, Togawa O, Baba M, Karasev E, Volkov YN, Omata N and Noriki S (2004) Lithogenic flux in the Japan Sea measured with sediment traps. *Marine Chemistry* **91**, 143–63.

Park S-U and Kim J-W (2006) Aerosol size distributions observed at the Seoul National University campus in Korea during the Asian dust and non-Asian dust periods. *Atmospheric Environment* **40**, 1722–30.

Paterson GA and Heslop D (2015) New methods for unmixing sediment grain size data. *Geochemistry Geophysics Geosystems* **16**, 4494–506.

Pei W, Wan S, Clift PD, Cai G, Zhao D, Zhang J, Jiao WQ, Ju M, Song Z and Li A (2023) Farming stimulated stronger chemical weathering in South China since 3.0 ka BP. *Quaternary Science Reviews* **307**, 108065.

Reimer PJ and Stuiver M (2016) Extended 14C data base and revised CALIB 3.0 14C age calibration program. *Radiocarbon* **35**, 215–30.

Sagawa T, Nagahashi Y, Satoguchi Y, Holbourn A, Itaki T, Gallagher SJ, Saavedra-Pellitero M, Ikehara K, Irino T and Tada R (2018) Integrated tephrostratigraphy and stable isotope stratigraphy in the Japan Sea and East China Sea using IODP Sites U1426, U1427, and U1429, Expedition 346 Asian Monsoon. *Progress in Earth and Planetary Science* **5**, 1–24.

Saito Y, Katayama H, Ikehara K, Kato Y, Matsumoto E, Oguri K, Oda M and Yumoto M (1998) Transgressive and highstand systems tracts and post-glacial transgression, the East China Sea. *Sedimentary Geology* **122**, 217–32.

Shen X, Wan S, France-Lanord C, Clift PD, Tada R, Révillon S, Shi X, Zhao D, Liu Y, Yin X, Song Z and Li A (2017) History of Asian eolian input to the Sea of Japan since 15 Ma: links to Tibetan uplift or global cooling? *Earth and Planetary Science Letters* **474**, 296–308.

Son H-Y, Park J-Y, Kug J-S, Yoo J and Kim C-H (2014) Winter precipitation variability over Korean Peninsula associated with ENSO. *Climate Dynamics* **42**, 3171–86.

Sone T, Kano A, Okumura T, Kashiwagi K, Hori M, Jiang X and Shen C-C (2013) Holocene stalagmite oxygen isotopic record from the Japan Sea side of the Japanese Islands, as a new proxy of the East Asian winter monsoon. *Quaternary Science Reviews* **75**, 150–60.

Steinke S, Glatz C, Mohtadi M, Groeneveld J, Li Q and Jian Z (2011) Past dynamics of the East Asian monsoon: no inverse behaviour between the summer and winter monsoon during the Holocene. *Global & Planetary Change* **78**, 170–77.

Sun X and Yang X (2005) Numerical modeling of interannual anomalous atmospheric circulation patterns over East Asia during different stages of an El Nino event. *Chinese Journal of Geophysics* **48**, 501–10.

Sun Y, Clemens SC, Morrill C, Lin X, Wang X and An Z (2012) Influence of Atlantic meridional overturning circulation on the East Asian winter monsoon. *Nature Geoscience* **5**, 46–49.

Tada R, Murray RW, Zarikian CA, Lofi Jr WT, Bassetti MA, Brace BJ, Clemens SC, Dickens GR, Dunlea AG and Gallagher SJ (2014) Asian Monsoon: onset and evolution of millennial-scale variability of Asian monsoon and its possible relation with Himalaya and Tibetan Plateau uplift. *Integrated Ocean Drilling Program Preliminary Reports* **346**.

Takahashi HG (2021) Long-term trends in snowfall characteristics and extremes in Japan from 1961 to 2012. *International Journal of Climatology* **41**, 2316–29.

Takano Y, Tachibana Y and Iwamoto K (2008) Influences of large-scale atmospheric circulation and local sea surface temperature on convective activity over the sea of Japan in December. *Sola* **4**, 113–16.

Tang Y, Wan S, Clift PD, Zhao D, Xu Z, Zhang J, Song Z, Jin H, Li M, Shi X and Li A (2022) Northward shift of the Northern Hemisphere westerlies in the early to late Miocene and its links to Tibetan uplift. *Geophysical Research Letters* **49**, e2022GL099311.

Wan S, Toucanne S, Clift PD, Zhao D, Bayon G, Yu Z, Cai G, Yin X, Révillon S and Wang D (2015) Human impact overwhelms long-term climate control of weathering and erosion in southwest China. *Geology* **43**, 439–42.

Wang H, Yu E and Song Y (2011) An exceptionally heavy snowfall in Northeast china: large-scale circulation anomalies and hindcast of the NCAR WRF model. *Meteorology & Atmospheric Physics* **113**, 11–25.

Wen X, Liu Z, Wang S, Cheng J and Zhu J (2016) Correlation and anti-correlation of the East Asian summer and winter monsoons during the last 21,000 years. *Nature Communications* **7**, 11999.

Yang S, Jiang S, Ling H, Xia X, Sun M and Wang D (2007) Sr-Nd isotopic compositions of the Changjiang sediments: implications for tracing sediment sources. *Science in China Series D: Earth Sciences* **50**, 1556–65.

Yoneda M, Uno H, Shibata Y, Suzuki R, Kumamoto Y, Yoshida K, Sasaki T, Suzuki A and Kawahata H (2007) Radiocarbon marine reservoir ages in the western Pacific estimated by pre-bomb molluscan shells. *Nuclear Instruments and Methods in Physics Research Section B: Beam Interactions with Materials and Atoms* **259**, 432–37.

Zhang N and Wang G (2020) Detecting the causal interaction between Siberian high and winter surface air temperature over northeast Asia. *Atmospheric Research* **245**, 105066.

Zhang W, Li H, Stuecker MF, Jin F-F and Turner AG (2016) A new understanding of El Niño's impact over East Asia: dominance of the ENSO combination mode. *Journal of Climate* **29**, 4347–59.

Zhao D, Wan S, Clift PD, Tada R, Huang J, Yin X, Liao R, Shen X, Shi X and Li A (2018) Provenance, sea-level and monsoon climate controls on silicate weathering of Yellow River sediment in the northern Okinawa Trough during late last glaciation. *Palaeogeography Palaeoclimatology Palaeoecology* **490**, 227–39.

Zhao D, Wan S, Lu Z, Zhai L and Li A (2020) Response of heterogeneous rainfall variability in East Asia to Hadley circulation reorganization during the late Quaternary. *Quaternary Science Reviews* **247**, 106562.

Zhao D, Wan S, Song Z, Gong X, Zhai L, Shi X and Li A (2019) Asynchronous variation in the Quaternary East Asian winter monsoon associated With the tropical Pacific ENSO-like system. *Geophysical Research Letters* **46**, 6955–63.

Zhao D, Wan S, Toucanne S, Clift PD, Tada R, Révillon S, Kubota Y, Zheng X, Yu Z and Huang J (2017) Distinct control mechanism of fine-grained sediments from Yellow River and Kyushu supply in the northern Okinawa Trough since the last glacial. *Geochemistry Geophysics Geosystems* **18**, 2949–69.

Zhao W, Sun Y, Balsam WL, Zeng L, Lu H, Otgonbayar K and Ji J (2015) Clay-sized Hf-Nd-Sr isotopic composition of Mongolian dust as a fingerprint for regional to hemispherical transport. *Geophysical Research Letters* **42**, 5661–69.

Zheng X, Li A, Wan S, Jiang F, Kao SJ and Johnson C (2014) ITCZ and ENSO pacing on East Asian winter monsoon variation during the Holocene: sedimentological evidence from the Okinawa Trough. *Journal of Geophysical Research: Oceans* **119**, 4410–29.

Zou J, Shi X, Zhu A, He L, Kandasamy S, Tiedemann R, Lembke-Jene L, Shi F, Gong X, Liu Y, Ikehara M and Yu P-S (2021) Paleoenvironmental implications of Sr and Nd isotopes variability over the past 48 ka from the southern Sea of Japan. *Marine Geology* **432**, 106393.